Engineering and testing a low-cost portable device for multispectral albedo measurement

Rihaan Sodhani

15 November 2025

Sr No.	Engineering and testing a low-cost portable device for multispectral albedo measurement using a novel dataset-based calibration approach	Page No.
SECTION 0 – Front Matter		
0.1	Title Page	1
SECTION 1 – Abstract and Keywords		
1.1	Abstract	3
SECTION 2 – Background, Problem & Ideation		
2.1	Introduction	3
2.2	Limitations of Existing Methods and Proposed Solutions	4
2.3	Genesis and Motivation	5
2.4	Literature Review	5
2.5	Engineering Goal	5
SECTION 3 – Planning & Methodology		
3.1	Project Planning and Approach	6
3.2	Detailed Methodology	6
3.3	System Design Documentation	10
3.4	User Manual	16
3.5	Ethics, Safety and Risk Assessment	16
SECTION 4 – Testing, Results & Evaluation		
4.1	Results and Observations	16
4.2	Analysis and Interpretation	19
4.3	Cost Feasibility and Design Justification	21
SECTION 5 – Discussion & Reflection		
5.1	Conclusion, Summary and Findings	23
5.2	Future Scope & Improvements	23
5.3	Impact on Society and Wider Application	24
5.4	Personal Learning Outcomes and Reflections	25
5.5	Challenges Faced and Problem-Solving Approach	25
SECTION 6 – References & Appendices		
6.1	Bibliography	25

Section 1

1.1 Abstract

The Urban Heat Island (UHI) Effect, characterised by the temperatures in urban zones being significantly higher than surrounding rural areas, is a severe problem in large cities. Albedo is the fraction of the incident radiation that is reflected from a surface. The UHI effect is driven primarily by the re-radiation of absorbed solar energy from low-albedo urban structures like pavements and roofing. Albedo is measured using albedometers, which are generally composed of two pyranometers and tend to be expensive and relatively unportable. In this project, the design of a low-cost, mobile albedometer is proposed, capable of measuring both broadband and spectral albedo, integrating orientation to ensure stable deployment. A calibration method for an outdoors environment is also developed using the ASTM (American Society for Testing and Materials) G-173 dataset. The device was validated by testing it on some surfaces of approximately known albedo, including copper, aluminium, concrete, and grass, and accurate albedo values were obtained. A micro scale analysis of the impact of albedo on Land-Surface Temperature (LST) was also carried out using copper and aluminium sheets, by graphing the temperature of the materials over the day. These findings were found to be comparable to the analogous Surface and Atmospheric UHI effects in real urban environments, highlighting the design's utility in UHI studies and materials research.

Keywords

Urban Heat Island (UHI) Effect, Albedometer, Multispectral Measurement, Narrow-to-Broadband (NTB) Calibration, Solar Irradiance

Section 2

2.1 Introduction

Around half the world's population is estimated to live in urban areas, making the problem of UHIs a pertinent one [4]. It contributes to poor air quality, elevated tropospheric ozone levels, increased heat-related illnesses and mortality rates, and raised energy consumption due to air conditioning use [34]. Infrastructure such as buildings and roads absorb and re-emit the sun's heat more than natural landscapes like forests and water bodies, forming a major contributing factor to UHIs [5].

The Surface Urban Heat Island (SUHI) refers to the difference in ground and object surface temperatures while the Atmospheric Urban Heat Island (AUHI) refers to the difference in air temperature between the urban and surrounding rural areas. During daytime, SUHI is at a maximum because urban surfaces absorb the sun's energy. From evening onwards, AUHI is at a maximum as these surfaces slowly release the heat stored [33]. This connects to another contributing factor to the UHI effect: emissivity (ε), which defines the ability of a material to emit energy [26]. To minimise the effect, urban surfaces should ideally have a high albedo, so most of the insolation is reflected rather than absorbed, and high emissivity, so that most of the heat is quickly emitted as longwave radiation rather than slowly released at night. This principle is tested at a micro scale in the project.

Albedo ranges from 0 to 1, where 0 refers to a blackbody, a theoretical medium that absorbs all the incident radiation, and 1 refers to an ideal reflector (an absolute white surface) in which all the energy falling on the surface is reflected [2]. Albedo is valuable in studies involving cool roofs, pavements, and vegetation for UHI mitigation, bifacial photovoltaic systems, and climate studies including glaciers, snow, and ice [6]. Spectral albedo refers to the reflectance in a given wavelength, while broadband albedo is calculated as an integral of the spectral reflectivity times the radiation, over all wavelengths in the visible spectrum. This project finds broadband albedo using this principle [2].

Different mitigation strategies, include preparing cool roofs and pavements by using high albedo paint or coatings [28], and green infrastructure, involving the addition of vegetation [27]. To quantify and monitor the health and cooling potential of these natural surfaces, the Normalized Difference Vegetation Index (NDVI) is widely used. It uses the difference between near-infrared (NIR) and red reflectance divided by their sum. Healthy vegetation strongly absorbs red light for photosynthesis while highly reflecting NIR light due to its leaf cell structure, resulting in high NDVI values +1. Conversely, unhealthy vegetation or impervious surfaces yield low NDVI values near 0 [31].

This paper first outlines the limitations of existing albedo measurement approaches and the motivation behind developing a low-cost, portable alternative. It then presents the conceptual framework of the proposed device, followed by a detailed description of the system design encompassing the electronics, programming, Computer-Aided Design (CAD), and calibration. The subsequent section describes the testing procedures, validation trials, and results obtained across different materials. This is followed by an analysis of the device's performance, cost feasibility, and design justification. The final section concludes by evaluating the broader implications of the work.

2.2 Limitations of Existing Methods and Proposed Solutions

Table 1: Limitations of existing methods and proposed solutions

No.	Limitation of Existing Methods	Proposed Solution
1	Generally, albedometers are composed of two pyranometers where one faces up and measures the global solar radiation, and the downfacing one measures the reflected solar radiation. Such devices can cost from ₹40,000 to over ₹1,00,000. The high cost makes it unfeasible for urban planners to study materials' albedo on a budget and limits deployment density.	By replacing the pyranometers with AS7341 spectrometers, price was reduced drastically to around ₹6,400, as shown in Table 4 in Section 3.5.5.
2	Pyranometer based systems are often heavy and relatively immobile, limiting their utility over a larger area.	The current design is small and lightweight, around $10cm \times 6cm \times 8cm$ in dimensions and weighing 86 g. This design thus boasts high mobility, allowing it to be easily mounted on an Unmanned Aerial Vehicle (UAV) or Unmanned Ground Vehicle (UGV), mounted on a tripod, or handheld for testing material properties.

No.	Limitation of Existing Methods	Proposed Solution
3	Pyranometers are broadband sensors, providing no information about the spectral distribution of reflected light. However, different materials, such as vegetation, snow, and ice, have distinct spectral signatures.	The AS7341 spectral sensors detect light across 8 channels in the visible spectrum (VIS), plus a near-infrared (NIR) and a clear channel [8]. This allows the device to measure multispectral albedo for detailed analysis.
4	Existing low-cost designs, such as those leveraging the AS7341 sensor, do not provide broadband albedo, the standard metric used in climate modelling [6]. Moreover, the existing narrow-to-broadband (NTB) conversion models, developed for satellite/high-altitude observation and large homogeneous zones, may not be suitable for downscaling [15].	Rather than relying on measurements from a costly spectroradiometer, requiring significant field data collection [9], this project uses a novel approach to calibrate the sensor and find broadband albedo using the ASTM G-173 dataset, a global standard for terrestrial solar irradiance, and the sensitivities of the AS7341 spectrometer. This technique of narrow-to-broadband (NTB) conversion is computationally less intensive and takes less time than calibration under real conditions.
5	The most commonly used albedo datasets, the MODIS Bidirectional Reflectance Distribution Function (BRDF), Nadir BRDF-Adjusted Reflectance (NBAR), and albedo products (MCD43) have a 500 m spatial resolution limit, despite the stated need of the ecological community for a product with finer resolution [7].	As this design can be mounted on a UAV or UGV or be used handheld, it can be used to analyse an area with a very fine resolution to address spatial heterogeneity.

2.3 Genesis and Motivation

I was introduced to the topic of Urban Heat Islands through school and from my own experience of oppressive temperatures in the city. This concern led me to investigate potential mitigation strategies, wherein the concept of albedo was emphasised due to its correlation with surface and air temperatures. However, any study on albedo would require expensive instruments to which I did not have access. Thus, designing a low-cost instrument was the first step towards any study involving UHIs.

2.4 Literature Review

During the literature review, I learnt about the inextricable link between albedo and urban heat islands, the albedo of pavements and roofing being the primary contributor to the effect [3]. Research revealed the high cost of most pyranometer-based albedometer systems as well. This demonstrated the need for an affordable device to measure reflectance.

I discovered some useful papers on designing low-cost multispectral albedometers. However, I came across several research gaps as well as mentioned in Section 2.2. Some standards on albedometer design were also noted for adherence in this project [10, 11].

2.5 Engineering Goal

The objective of this project is to design and validate a cost-effective, mobile multispectral albedometer prototype that overcomes the limitations of traditional pyranometer systems by integrating a compact AS7341 spectral sensor array and an ADXL345 accelerometer for orientation to ensure level testing, and that bypasses the difficulty of traditional calibration by using a novel approach based on the ASTM G-173 dataset and the sensitivities of the spectrometer bands.

Section 3

3.1 Project Planning and Approach

I began with ideation. Early ideas including using UAVs to generate heat maps, but the literature review revealed that most meaningful analysis of the UHI effect necessitated measuring reflectivity, leading to the idea of developing an albedometer design.

I decided to begin the project by working on the electronics, followed by programming and Computer-Aided Design (CAD) 3D printing. Throughout the process, regular informal testing was carried out in a terrace to ensure that progress was being made. Formal validation and testing on different materials formed the end of the project.

3.2 Detailed Methodology

3.2.1 Electronics

2 Adafruit AS7341 spectral sensors, which detect light across 8 channels in the visible spectrum (VIS), plus a near-infrared (NIR) and a clear channel have been used [8], one facing up to measure incident light and the other facing down to measure light reflected off a surface. Thus, a TCA9584 I^2C Multiplexer (MUX) has to be included as well. To ensure level deployment, especially during handheld or UAV testing, the design also includes an ADXL345 accelerometer, which measures orientation in terms of pitch and roll, indicating tilt to the sensor plane. These components are connected using I^2C communication protocol. An ESP32C3 microcontroller has been used in the design. Along with a rechargeable 3.7V 1250mAh LiPo battery as a power source, a switch was also included to allow the device to be turned on and off. A connection diagram has been shown in Figure 2 in Section 3.3.1.

3.2.2 Programming

Each component was programmed individually before the code was combined together near the end of the project. Since the sensor produced some light itself and experienced noise, dark calibration was deemed necessary. The program uploaded on the microcontroller sends the data collected JavaScript Operation Notation (JSON) format through wi-fi to a webpage built using Hypertext Markup Language (HTML). There, spectral albedo across the 8 VIS channels, the NIR channel, and the clear channel as well as an overall broadband albedo are displayed in real-time. A flowchart for the code is shown in Figure 3 in Section 3.3.2.

3.2.3 Computer-Aided Design

A CAD model of the albedometer was made on SolidWorks software. It consists of two halves, a central plate on which some electronic components are fixed, and a support with the

possibility of connecting a nut. Two diffusors were designed separately as domes. The body was 3D printed using white polylactic acid (PLA), and the diffusors was printed using transparent polycarbonate (PC). Images of the components' CAD models are shown in Figures 4-8 in Section 3.3.3.

3.2.4 Calibration

Broadband albedo

Initial attempts at calibration to estimate a broadband albedo involved simply dividing the sum of the readings from the upward facing spectral sensors by the sum of the readings from the downward facing sensors. However, this technique was deemed ineffective as it failed to match the expected values for common materials like copper. It fails for the following reasons:

(1) It is limited to specific wavelength bands detected by the AS7341 sensor;
(2) It fails to account for varying responsivity of the sensor; and
(3) It fails to account for varying energy contributions of photons across the spectrum. Since $E = \frac{hc}{\lambda}$ (where E and λ are the photon's energy and wavelength respectively, h is Plank's constant, and c is the speed of light in vacuum), photons of violet light having lower wavelength are more energetic than photons of red light [14].

Thus, more sophisticated Narrow-to-Broadband (NTB) conversion was necessary. The existing narrow-to-broadband (NTB) conversion models, developed for satellite/high-altitude observation and large homogeneous zones, may not be suitable for downscaling [15]. On the other hand, regression models require simultaneous measurements with a reference spectroradiometer, an expensive lab-grade equipment, requiring significant field data collection [9]. Moreover, this can introduce systematic error due to potential errors in the reference instrument, which can be caused by aging. To address this problems, I implemented a new physics-based calibration technique using the American Society for Testing and Materials (ASTM) G-173 dataset. Similarly to regression techniques, weight coefficients were found for the spectral albedo provided by the AS7341 sensor bands [15]. However, the dataset provides a standard for the ideal, clear-sky power distribution (watts per square meter per nanometre of bandwidth) of insolation [16], bypassing the need for land-based calibration. The specified atmospheric conditions are the following:

(1) The 1976 U.S. Standard Atmosphere with temperature, pressure, aerosol density (rural aerosol loading), air density, molecular species density specified in 33 layers
(2) An absolute air mass of 1.5 (solar zenith angle 48.19°)
(3) Angstrom turbidity (base e) at 500 nm of 0.084c
(4) Total column water vapor equivalent of 1.42 cm
(5) Total column ozone equivalent of 0.34 cm
(6) Surface spectral albedo (reflectivity) of light soil as documented in the Jet Propulsion Laboratory ASTER Spectral Reflectance Database [16].

This technique has certain limitations as well. Most significantly, the assumptions made by the dataset limit the effectiveness of this device under cloudy conditions. To correct for the characteristics of the AS7341 sensor, information from the manufacturer's datasheet were also integrated [8]. A detailed description of this calibration technique is included below.

The dataset was loaded as a pandas DataFrame in a Python environment on Google Colab [17]. A visualisation of the ASTM G173 dataset, created using matplotlib, is shown in Figure 1.

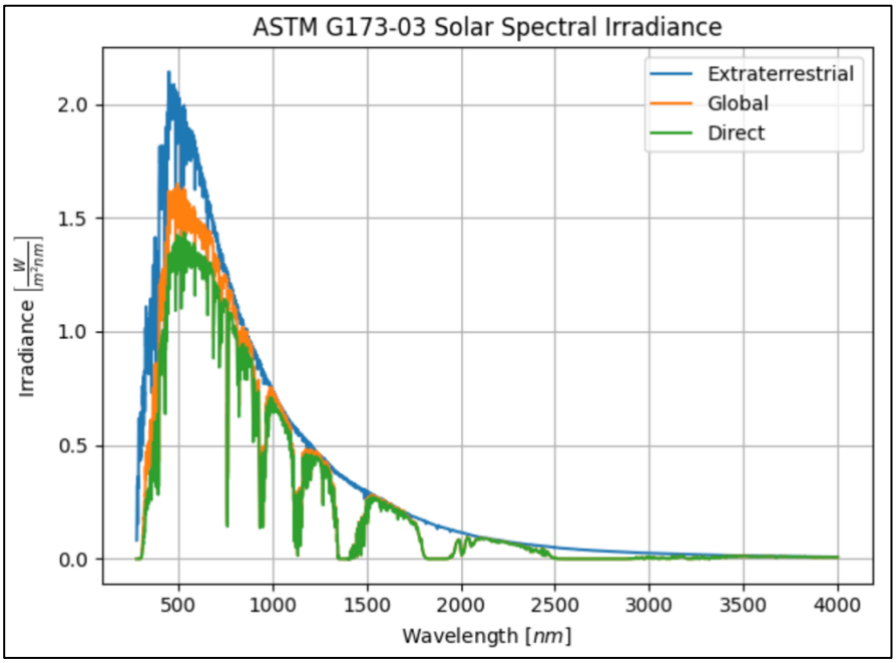


Figure 1: A visualisation of the ASTM G-173 dataset

The "Global" column was used as it represents the total solar irradiance incident on a surface under standard atmospheric conditions, accounting for both direct and diffuse components of sunlight [18]. To appropriately represent each AS7341 spectral band's contribution to the overall solar irradiance, a Gaussian weighting model was applied to the standard ASTM G-173 global solar spectrum. The central wavelength and Full-Width at Half-Maximum (FWHM) of each AS7341 channel were obtained from the manufacturer's datasheet [8].

The spectral response of each channel i, where $i \in \{1, 2, 3, 4, 5, 6, 7, 8, 9\}$ (1-8 represent the 8 VIR channels, and 9 represents the NIR channel), was modelled as a Gaussian function $R_i(\lambda)$ centred at its nominal wavelength λ_i, having a Full-Width at Half-Maximum $FWHM_i$ and a standard deviation σ_i. The CLEAR channel was not included in calculating broadband albedo as measures the total incident light intensity across the entire visible and near-infrared spectrum without spectral filtering. The constant coefficient $\frac{1}{\sigma\sqrt{2\pi}}$ was excluded as the $R_i(\lambda)$ is normalised, so that $max(R_i) = 1$. The normalised Gaussian function is defined below [19].

$$R_i(\lambda) = e^{\left[-\frac{1}{2}\left(\frac{\lambda-\lambda_i}{\sigma_i}\right)^2\right]}$$

where standard deviation can be expressed in terms of FWHM as shown below [19].

$$\sigma_i = \frac{FWHM_i}{2\sqrt{2ln(2)}}$$

$E(\lambda)$ was defined as the value of the Global irradiance (in $\frac{W}{m^2 nm}$) at λ in the ASTM G-173 dataset. The product of this response with the ASTM G-173 spectral irradiance was integrated over wavelength to determine the effective energy captured by that band [15]. The integral associated with each channel i, I_i, was found as shown below, where the integration was computed using the trapezoidal rule.

$$I_i = \int_{\lambda_{min}}^{\lambda_{max}} E(\lambda) R_i(\lambda) d\lambda$$

where $\lambda_{min} = 280.0\,nm$ and $\lambda_{max} = 4000.0\,nm$, the limiting wavelengths of the dataset at which responsivity of the channels is zero. Based on the dataset, the width dλ is 0.5nm. Finally, the weights ascribed to each channel, W_i, were found by normalising the integrals, so that $\sum_{i=1}^{9} W_i = 1$.

$$W_i = \frac{I_i}{\sum_{i=1}^{9} I_i}$$

The weights found are included in Table 2 in Section 3.3.4. These weights were then applied to find broadband albedo from spectral albedo α_i using the following formula.

$$\alpha_{broadband} = \sum_{i=1}^{9} W_i\,\alpha_i$$

Diffusors

Dome-shaped diffusors were 3D printed using transparent polycarbonate. The dome was found to consistently decrease an AS7341 sensor's readings during testing. However, the transmittance (the fraction of light that passes through) of the polycarbonate dome is probably not constant across all wavelengths [20]. Thus, to ensure that the values displayed are accurate, the device was calibrated to minimise the impact of the diffusor on the wavelength of incident light.

Readings were taken for white PLA, black PLA, and copper both with and without the diffusor. They were taken under artificial light as it was easier to control the amount of incident light. Since it was the raw readings of the AS7341 sensors and not albedo that was being corrected, natural light was not deemed necessary. Then, a linear regression model ($y = mx + c$) was developed for each of the 10 bands to map the readings with a diffusor to those without a diffusor. However, the first models had negative y-intercepts, resulting in negative values under certain light conditions. Thus, the intercepts were fixed at the origin ($y = mx$) and the adjusted readings were used to calculate albedo. The models used and their coefficients of determination are shown in Section 3.3.4.

3.2.5 Validation and Testing

First, the device was validated informally by testing it on black and white surfaces. It consistently displayed low readings for dark surfaces and high readings for light surfaces in natural light. For formal validation and testing, first, the device was used to find the broadband albedo for certain surfaces, including copper and aluminium sheets, a concrete road, and grass in a park near my home. These were compared to approximately known albedo values [32]. The cost of obtaining pure white reference standards, such as Spectralon or Barium Sulphate paint, was deemed too high for a project focused on a low-cost design, resulting in this focus on common materials.

Second, $15cm \times 15cm$ copper and aluminium sheets were placed out in the sun for a day, resting on carboard for insulation. The temperatures of the surface temperature of the two materials were recorded at regular 1 hour intervals from 11:00 to 18:00. 3 readings were taken per data point to minimise random error caused by shaking of my hand while measuring. A GM320S digital infrared thermometer was used due to availability. However, the thermometer has a fixed emissivity setting of 0.95, while metals have a much lower emissivity (aluminium from 0.05 to 0.07, while copper ranges from 0.01 to 0.07) [22]. Thus, using the thermometer would lead to systematically lower readings for temperature. To fix this problem, a $1cm \times 1cm$ piece of masking tape, which has an emissivity of around 0.92 [23], was stuck on the surface

of each of the metals. It reaches the same temperature as the surface of the metal beneath it, providing an accurate proxy for the temperature of the metal. The graphs plotted were then used for micro scale analysis of the impact of albedo on Land-Surface Temperature (LST). The results of the validation and testing is shown in Section 4.1.

3.3 System Design and Documentation

3.3.1 Electronics

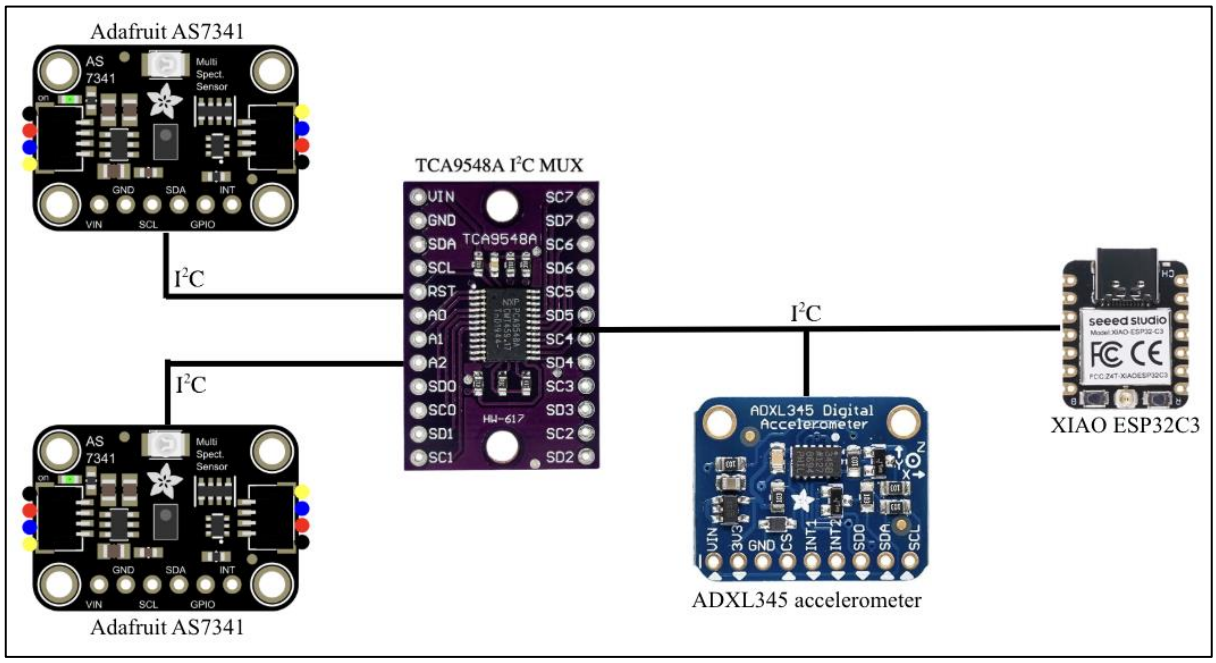


Figure 2: Connection diagram of the designed system

3.3.2 Programming

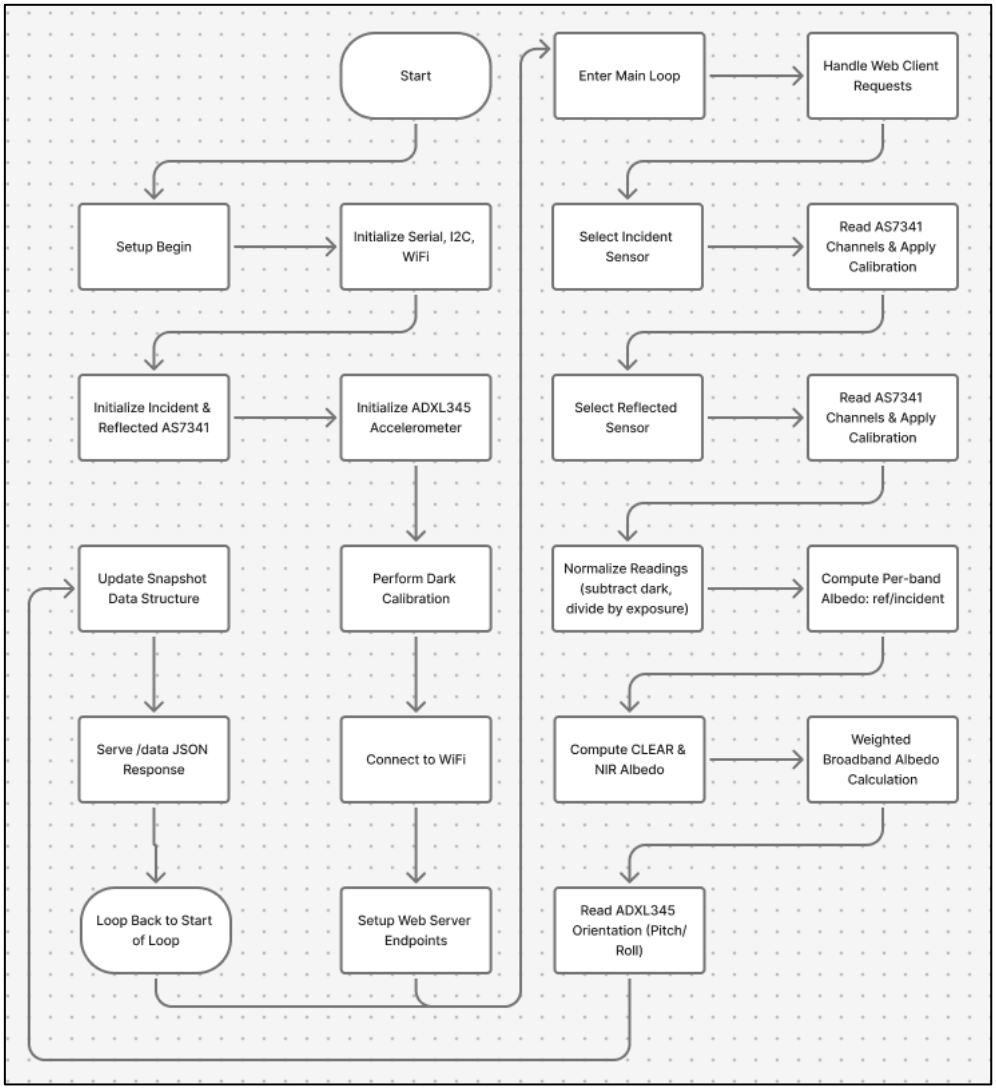


Figure 3: Flowchart for the code

3.3.3 Computer-Aided Design

The dimensions of the design are around $10cm \times 6cm \times 8cm$. It weighs 86 g. The design is dust proof. PLA was used for 3D printing as the model is a prototype. Ideally, the design should be printed in Acrylonitrile Styrene Acrylate (ASA) as it resistant to sunlight [35].

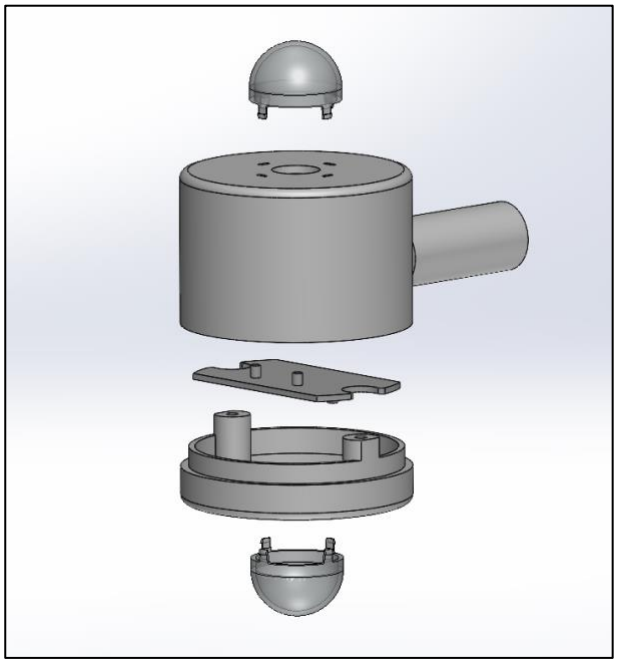


Figure 4: Exploded view of the albedometer's CAD model

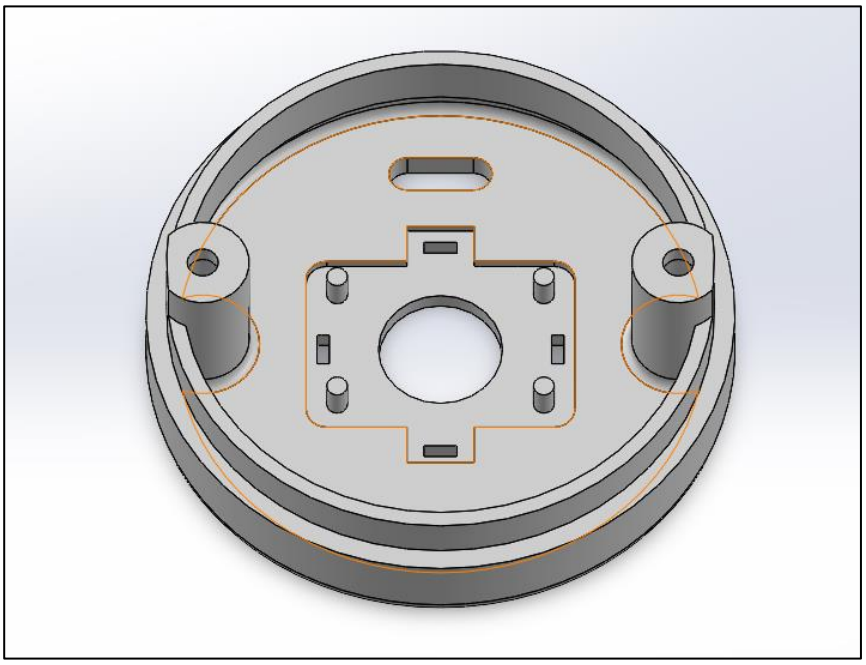


Figure 5: CAD model of the top piece of the albedometer's body

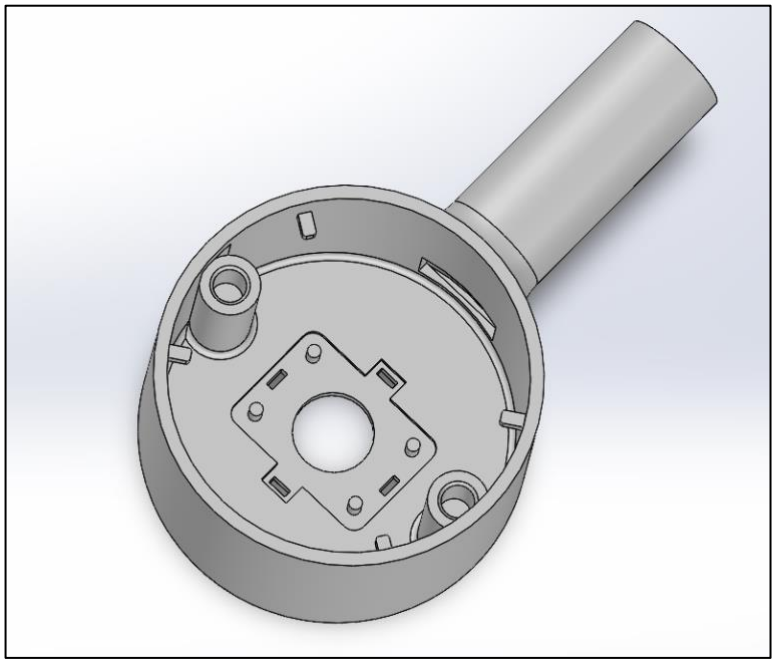


Figure 6: CAD model of the bottom piece of the albedometer's body

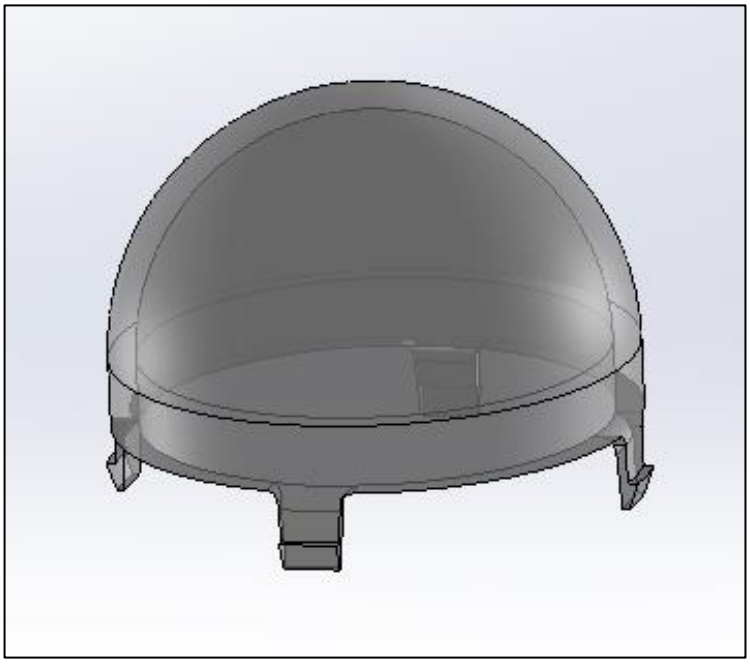


Figure 7: CAD model of the diffusor

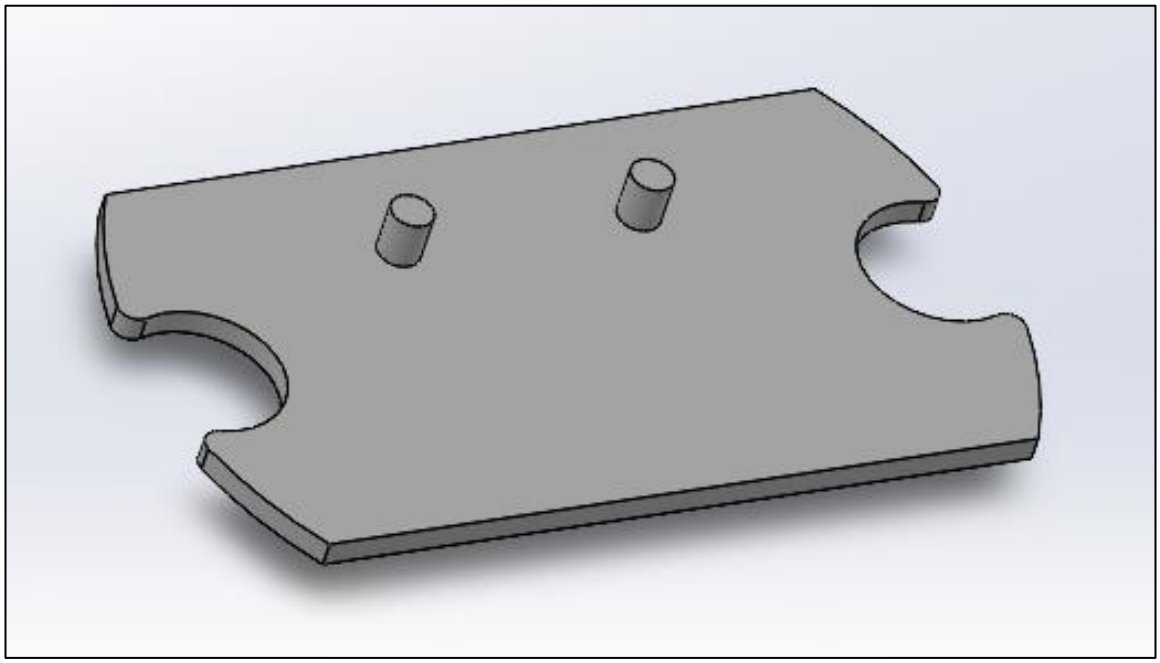


Figure 8: CAD model of the plate embedded in the albedometer

3.3.4 Calibration

The techniques by which these values are found are included in Section 3.2.4. An analysis of all the values obtained is included in Section 4.3.1.

Broadband albedo

Table 2: The weights used to find broadband albedo

No.	Centre wavelength of channel / nm	Weight
1	415	0.0734
2	445	0.0879
3	480	0.0975
4	515	0.0950
5	555	0.0952
6	590	0.0919
7	630	0.0892
8	680	0.0842
9	910 (NIR)	0.2856

Diffusors

Table 3: The linear regression models with intercepts fixed at origin used to minimise diffusor bias

No.	Centre wavelength of channel / nm	Scale Factor m	Coefficient of Determination R^2
1	415	1.9053	0.968
2	445	1.69827	0.9874
3	480	1.81799	0.9837
4	515	1.71893	0.9833
5	555	1.76909	0.9867
6	590	1.88224	0.9814
7	630	1.85001	0.9829
8	680	1.65001	0.9833
9	910 (NIR)	1.81739	0.97

3.3.5 Bill of Materials

The total cost included is an estimate.

Table 4: Bill of materials

No.	Designator	Component	Qty	Unit Cost	Total Cost	Source of Material
1	XIAO ESP32C3	microcontroller	1	₹504	₹504	t.ly/AmKWo
2	AS7341	Spectral sensor	2	₹2,195	₹4,390	t.ly/3lQGK
3	ADXL345	Accelerometer	1	₹123	₹123	t.ly/ZYAY6
4	TCA9548A	I^2C MUX	1	₹75	₹75	t.ly/LRJri
5	SPST Rocker Switch	Switch	1	₹25	₹25	t.ly/hO500
6	WLY853837	LiPo Battery	1	₹413	₹413	t.ly/gDHSQ
7	3D printing–white PLA filament and transparent PC filament	Structural	1	₹380	₹380	N/A
8	Glue Sticks, Wires, Solder Wire, Nut Bolts, Screws,	Consumables	1	₹500	₹500	N/A

	Inserts, Heat Shrinks, etc					
Total			9	₹6,410		

3.4 User Manual

The code must first be updated with the wi-fi Service Set Identifier (SSID) and password that the user needs. If the wi-fi is unavailable, the device will set up its own wi-fi, "AlbedoRig," to which the user must connect. Then, it can be uploaded onto the microcontroller through a C-type cable. The Serial Monitor will display an Internet Protocol (IP) address that must be inputted onto the HTML webpage, followed by pressing "Save" and "Start" to begin receiving information. To dark calibrate, the albedometer must be removed from all light; for example, it can be placed in a dark drawer or inside a black bag. Then, the user must press "Dark Cal" button on the webpage and wait for a message indicating the completion of the dark calibration. To use the albedometer, it must be held or mounted in a perfectly horizontal configuration, with both pitch and roll less than 3°. To get a stable reading, it is recommended to use a stand such as a tripod. Pressing the "Save Log (.txt)" button saves the data recorded in the form of a text (txt) file.

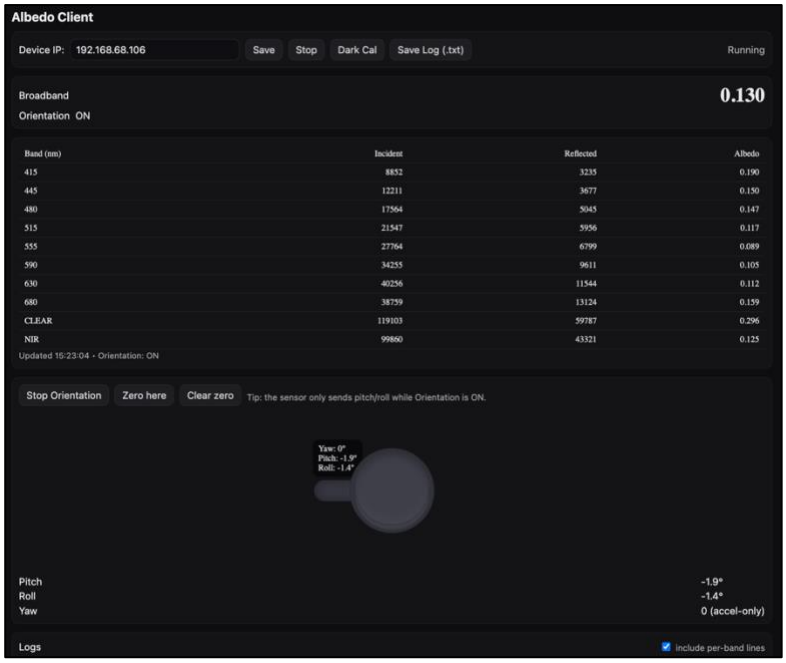


Figure 9: Webpage for the albedometer

3.5 Ethics, Safety, and Risk Assessment

This project does not involve any significant ethical, safety, or risk issues. All components are secured inside a 3D printed casing and the voltage involved is low (3.3V).

Section 4

4.1 Results and Observations

Table 5: Multispectral and broadband albedo for copper

Band	**Raw reading of incident light = I**	**Raw reading of reflected light = R**	**Albedo = R/I**
415 nm	1965	1321	0.672
445 nm	2968	2073	0.698
480 nm	4167	2849	0.684
515 nm	4808	3343	0.695
555 nm	5504	3652	0.663
590 nm	5598	4021	0.718
630 nm	6373	4718	0.740
680 nm	6933	5514	0.795
CLEAR	18469	16745	0.907
915 nm (NIR)	7953	6919	0.870
Broadband			0.754

Table 6: Multispectral and broadband albedo for aluminium

Band	**Raw reading of incident light = I**	**Raw reading of reflected light = R**	**Albedo = R/I**
415 nm	1919	1477	0.770
445 nm	2896	2323	0.802
480 nm	4065	3210	0.790
515 nm	4696	3752	0.799
555 nm	5369	4089	0.762
590 nm	5460	4470	0.819
630 nm	6210	5232	0.843
680 nm	6758	6040	0.894
CLEAR	18017	18578	1.031
915 nm (NIR)	7823	7352	0.940
Broadband			0.846

Table 7: Multispectral and broadband albedo for concrete

Band	**Raw reading of incident light = I**	**Raw reading of reflected light = R**	**Albedo = R/I**
415 nm	28100	3552	0.126
445 nm	43298	5217	0.120
480 nm	58634	7321	0.125
515 nm	65219	9324	0.142
555 nm	65535	10930	0.167
590 nm	65535	12044	0.184
630 nm	65535	13942	0.213
680 nm	65535	15246	0.233
CLEAR	65535	49959	0.762
915 nm (NIR)	65535	20817	0.318
Broadband			0.208

Table 8: Multispectral and broadband albedo for grass

Band	**Raw reading of incident light = I**	**Raw reading of reflected light = R**	**Albedo = R/I**
415 nm	3918	520	0.133
445 nm	5772	612	0.106
480 nm	7757	640	0.083
515 nm	8701	924	0.106
555 nm	9526	1010	0.106
590 nm	9678	1048	0.108
630 nm	10594	940	0.089
680 nm	11385	1121	0.099
CLEAR	39881	9871	0.248
915 nm (NIR)	19394	10641	0.553
Broadband			0.231

Table 7: Temperatures recorded for copper and aluminium over the day

Time of day	Copper temp. 1 (±0.1) / °C	Copper temp. 2 (±0.1) / °C	Copper temp. 3 (±0.1) / °C	Aluminium temp. 1 (±0.1) / °C	Aluminium temp. 2 (±0.1) / °C	Aluminium temp. 3 (±0.1) / °C
11:00	25.3	26.1	25.8	25.5	26.5	26.1
12:00	27.4	27.2	27.3	27.3	27.6	27.6
13:00	29.9	30.7	30.5	28.9	29.6	29.5
14:00	36.6	36.4	36.3	33.2	32.4	33
15:00	31.2	32.5	31.2	31.3	31.8	31.7
16:00	33	34.2	33.1	32.4	31.9	33.2
17:00	28.4	28.4	28.4	28.9	28.8	28.8
18:00	27.9	28	26.7	28	28.2	28

4.2 Analysis and Interpretation

4.3.1 Calibration Results

Broadband albedo

The most significant observation from Table 2 is the large weight (0.2856) assigned to albedo of the NIR region, centred at 910 nm, as compared to the other bands. This high weight is entirely justified because the Near region contains approximately 50% of the total shortwave solar energy incident on the Earth's surface [21]. This suggest that materials (like cool roofing paints) designed to reflect NIR energy, while appearing the same colour to the human eye, will register a higher albedo value and are thus predicted to have a greater impact in mitigating the UHI effect.

Diffusors

Displayed in Table 3, The coefficient of determination R^2 values across all nine channels are exceptionally high, ranging from 0.968 to 0.9874. This high correlation validates that the diffuser introduces a consistent and predictable systematic error (a proportional scaling factor m), and confirms that a simple linear regression model is highly effective for correcting this bias across the entire visible and NIR spectrum.

It is observed that the values of m vary across wavelengths. Transmittance, which is inversely proportional to m, is highest for 615 nm (red), with $m = 1.65001$, and lowest for 415 nm (violet), with $m = 1.9053$. Variations in attenuation are due to characteristics of the PC diffusors themselves. This clear spectral dependency proves that a single, average correction factor would introduce significant colour bias (i.e., systematically over-correcting the NIR and under-correcting the blue).

4.3.2 Testing and Validation Results

Table 8: Measured vs literature values for broadband albedo

No.	Surface	Measured albedo	Literature albedo
1	Copper	0.754	0.74 [32]
2	Aluminium	0.846	0.85 [32]
3	Concrete	0.208	0.25-0.35 [32]
4	Grass	0.231	0.15-0.25 [32]

For broadband albedo, copper (0.754) and aluminium (0.846) were found to be exceptionally close to the literature values (0.74 and 0.85, respectively), off by around 1.89% and 0.47%, respectively. This is probably because the sheets were new and polished. The broadband albedo of concrete (0.208) was found to be slightly lower than literature values (0.25-0.35), off by around 30.67% from the average of the range (0.30). Since this test was done on an actual road, this difference can be attributed to age and variation in composition. The broadband albedo of grass in a park near my house (0.231) was found to fall within the literature range (0.15-0.25). Generally, this validation corroborates the accuracy of the design. The readings for grass have also been used to estimate the Normalised Difference Vegetation Index (NDVI).

$$NDVI = \frac{\alpha_{NIR} - \alpha_{red}}{\alpha_{NIR} + \alpha_{red}} \approx \frac{\alpha_{NIR} - \alpha_{680\,nm}}{\alpha_{NIR} + \alpha_{680\,nm}} \approx \frac{0.553 - 0.099}{0.553 + 0.099} \approx +0.696$$

A value like +0.696, closer to +1.0, indicates healthy vegetation [31]. For comparison, NDVI has also been computed for concrete.

$$NDVI = \frac{0.318 - 0.233}{0.318 + 0.233} = +0.154$$

This value is also consistent with the meaning of NDVI. For a vegetation-free material like concrete, it should be closer to 0 [31].

To process the data for temperatures recorded for copper and aluminium over the data, first, mean temperature for copper and aluminium were found. Then, the uncertainty due to random error (variations among readings) and the uncertainty due to systematic error (least count of the digital IR thermometer) were computed. The latter is always ±0.1°C. The larger in magnitude among these two values is then used. Processing of the first data point for copper has been shown as an example.

$$T_{Cu} = \frac{25.3°C + 26.1°C + 25.8°C}{3} \approx 25.7°C\ (to\ 1\ d.p.)$$

$$\Delta T_{Cu} = \frac{26.1°C - 25.3°C}{2} = \pm 0.4°C$$

The data in the table has been shown accurate to 1 decimal point, consistent with the original readings.

Table 9: Processed data for temperatures recorded for copper and aluminium over the day

Time of day	**Mean copper temp. T_{Cu} / °C**	**Mean aluminium temp. T_{Al} / °C**	**ΔT_{Cu} / °C**	**ΔT_{Al} / °C**
11:00	25.7	26.0	±0.4	±0.5
12:00	27.3	27.5	±0.1	±0.2
13:00	30.4	29.3	±0.4	±0.4
14:00	36.4	32.9	±0.2	±0.4
15:00	31.6	31.6	±0.7	±0.3
16:00	33.4	32.5	±0.6	±0.7
17:00	28.4	28.8	±0.1	±0.1
18:00	27.5	28.1	±0.7	±0.1

Using these data points and uncertainties (for error bars), a graph has been plotted for micro scale analysis of the impact of albedo on Land-Surface Temperature (LST).

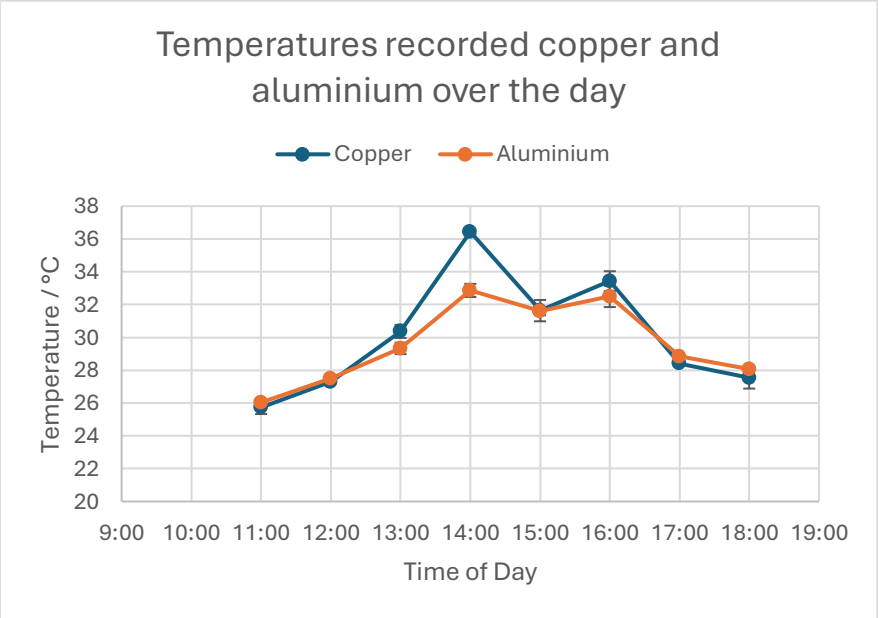


Figure 10: A graph showing the temperatures recorded for copper and aluminium over the day

It is observed that both copper and aluminium display clear diurnal patterns. Their temperatures rise from morning to reach a peak around noon and then continue to decline into the evening. These behaviours mirror fundamental principles of SUHI and AUHI dynamics. Between 11:00 and 14:00, both materials show a steady rise in temperature as solar irradiance increases, contributing to an increase in surface temperature. From the 16:00 onwards, temperatures decline as the surfaces emit their heat into the surroundings, contributing to an increase in air temperature. These changes are analogous to an increase in the SUHI and AUHI effect, respectively, in an actual urban environment. An anomalous observation is the fall in temperature at 15:00, which subsequently rises again. This can probably be attributed to a short-term change in environmental conditions, such as cloud cover.

Aluminium, having a higher broadband albedo (0.846), reflects a greater fraction of incident solar radiation than copper (0.754). This is consistent with the observation that aluminium exhibits a less sharp rise and lower peak temperatures at 14:00. A third notable observation is the fact that the temperature of copper falls below that of aluminium in the evening from 17:00 onwards. This is likely attributable to the fact that the aluminium sheet has a lower emissivity than the copper sheet, so it releases stored heat less efficiently [30]. This test shows the effectiveness of the design in fine-resolution UHI studies and materials research. To minimise the UHI effect, a material should have high albedo and emissivity.

4.3 Cost Feasibility and Design Justification

The estimated cost of the prototype is around ₹6,400, as shown below. Scaling up and producing more devices could lower the cost further. This excludes any components used for mounting such as tripods, UAVs, or UGVs. The device can also be handheld, which requires no additional components. This is significantly cheaper than other designs in literature, which reach around $180 [6] (around ₹16,000), as well as commercial albedometers, which cost from ₹40,000 to over ₹1,00,000.

Table 10: Design Justification

No.	Feature/Component	Justification
1	AS7341 spectral sensors	It is relatively low in cost, readily available, and employed in existing literature [6].
2	TCA9548A I^2C MUX	It allows a single I^2C bus to communicate with both sensors [13], important as the two AS7341 sensors have a fixed, common I^2C address.
3	ADXL345 accelerometer	It is inexpensive and measures only pitch and roll; yaw was not deemed important for this project as rotation about the vertical/Z axis will not affect the albedometer's reading as long as it is horizontal.
4	I^2C communication protocol	It was necessitated by the AS7341 sensor and employed in existing literature [6]. High speed communication was not essential in the albedometer.
5	XIAO ESP32C3 microcontroller	The integrated wi-fi allows collected data to be transmitted directly rather than being stored, allowing for real-time visualisation, logging and analysis. Moreover, the C3 is designed for low power operation, maximising battery life for long-term deployment [12].
6	White PLA filament 3D printed body	White has high reflectivity and diffusely reflects light, preventing the body from

		absorbing and re-emitting light, which introduces bias in the AS7341 readings. This is consistent with official standards like the ISO 9060 [10].
7	Dome-shaped transparent PC 3D printed diffusor	Without a diffusor, a flat sensor's response is highly sensitive to the angle at which light strikes its surface. A cosine diffusor scatters the incoming light equally from all directions. The diffusor also shields the AS7341 sensor from the environment [10, 11]. The material and shape is consistent with existing literature [6].

Section 5

5.1 Conclusion, Summary and Findings

This project successfully designed, constructed, and validated a portable, low-cost multispectral albedometer capable of measuring spectral and broadband albedo using dual AS7341 sensors and an integrated ADXL345 accelerometer for stable deployment. It is intended for use in studies involving the Urban Heat Island (UHI) effect.. The device addressed key limitations of existing pyranometer-based systems by significantly reducing cost, improving mobility, and permitting detailed multispectral analysis, such as measuring the Normalised Difference Reflectivity Index (NDVI) of vegetation, an indicator of plant health and evapotranspiration rate [31]. A novel dataset-based calibration method, based on the ASTM G-173 solar spectrum and the AS7341 sensor responsivity across bands, was developed to convert narrowband reflectance measurements into the broadband albedo used in most climate studies [6]. This calibration approach eliminated the dependence on expensive reference instruments and extensive measurements, while maintaining consistency with theoretical expectations. Linear regression models were also developed and integrated to minimise spectral bias due to the diffusors.

Testing on surfaces like copper, aluminium, cement, and grass resulted in broadband albedo values generally consistent by those predicted by literature. The values of the weights themselves resulted in valuable inferences. For example, the higher weight for NIR albedo (0.2856) suggests that an urban surfaces that reflect more light in this region of the spectrum, while appearing the same to the human eye, would be effective at mitigating the UHI effect. A micro scale analysis of the effect of albedo on Land-Surface Temperature (LST) was carried out using copper and aluminium, measuring the temperature of the surfaces at regular intervals. The clear diurnal pattern of temperatures was related to the albedo and emissivity of the two materials, as well as the analogous Surface and Atmospheric UHI effects. They indicated that aluminium had a higher albedo (consistent with measurements) and lower emissivity (consistent with literature [30]) than copper. This shows the design’s effectiveness in fine-resolution UHI studies and materials research. A limitation is the clear-sky assumption made by the dataset, reducing effectiveness under cloudy conditions.

5.2 Future Scope and Improvements

There are a certain of avenues through which the scope of this project could be expanded or the methodology improved.

(1) **Comparison with an industrial albedometer:** Weights for the albedo of each band could be found using regression by comparing against an industrial, pyranometer-based albedometer. These could be compared with the weights found using the dataset-based calibration technique for further validation.
(2) **Addition of Environmental Sensors:** Addition of surface and air temperature sensors [24] and a humidly sensor [6] would increase the device's usefulness in a detailed study on UHIs. The correlation of air temperature with albedo is not studied extensively yet.
(3) **Correction for different atmospheric conditions:** A significant limitation of the current design is the clear-sky assumption of the ASTM G-173 dataset. The device could be manually tested under different atmospheric conditions and calibrated to generally correct for this error.
(4) **Measuring Emissivity:** A contact temperature sensor could be used along with readings in the NIR band to estimate the emissivity of a surface [25]. Low emissivity materials slowly radiate the heat absorbed in the dark, intensifying the UHI effect.
(5) **Testing stability:** The device could be tested deployed using UAVs and UGVs, with added auto-correction for instability using the ADXL345 accelerometer.
(6) **Comparison of UHI mitigation strategies:** Different mitigation strategies, such as green infrastructure, involving the addition of vegetation [27], and preparing cool roofs by using high albedo paint or coatings [28], could be compared and evaluated quantitatively for a low cost using this design. The design is particularly useful for green infrastructure as it can be used to calculate the Normalised Difference Vegetation Index (NDVI). It is also useful for cool materials design because of the weights calculated based on real physics rather than regression.
(7) **Broader spectrum:** The AS7341 sensor, which ranges from around 415 nm to 915 nm (centres of the bands), does not include as broad of a spectrum as a pyranometer albedometer, which often range from around 285 nm to 3000 nm. A shortwave infrared (SWIR) sensor could be integrated to look at a broader spectrum, enhancing the device's accuracy.

5.3 Impact on Society and Wider Application

The Urban Heat Island effect negatively impacts the estimated 4.7 billion people living in urban areas, as of 2024 [4], increasing energy consumption and heat-related illness and death [34]. The albedo of urban surfaces such as roofs and pavements is a major contributing factor to this problem. However, essential study of UHIs is inhibited by the high cost of meteorological equipment such as pyranometers. This device helps democratise albedo measurement by replacing expensive equipment with open-source, low-cost hardware. The cost is drastically decreased from ₹40,000 to over ₹1,00,000 for traditional albedometers to an estimated ₹6,400 for this design. The design is also much lighter and smaller than commercial devices. The mobility and affordability allows large-scale deployment for urban planning as well as community-scale citizen science. Moreover, the novel calibration method significantly decreases time and effort spent on calibrating the equipment against another device, allowing faster deployment. By informing urban developers, more accessible UHI data can allow quantitative comparison of different mitigation strategies, thus reducing thermal stress and energy consumption due to the UHI effect, promoting sustainability in the long run. The small scale/high resolution and mobility of the device allows rapid assessment of materials in-situ as

well as detailed microclimate modelling that accounts for spatial heterogeneity. In the field of energy, the device can be used to ensure that high albedo surfaces are used surrounding bifacial photovoltaic (PV) systems, which capture direct sunlight from the front and reflected light form the ground surface on the rear, to boost efficiency in power generation, producing 5-30% more power than ordinary PV systems [29].

Spectral albedo is essential for the development of new materials, paints, and coating to mitigate the UHI effect. For example, the weights for the albedo of each band obtained in Table 2 suggest that a material that looks the same to the human eye but reflects a large amount of NIR light would have a major impact on controlling the UHI effect, because of the larger weight ascribed to the NIR band. However, devices that measure spectral albedo tend to be very complex or expensive, and a traditional pyranometer-based system measures only broadband albedo. This project provides an accessible solution to this problem. The spectral sensors can also be used to find the Normalized Difference Vegetation Index (NDVI). This allows it to simultaneously evaluate the effectiveness of green infrastructure as a UHI mitigation strategy and quantify its health, density, and evapotranspiration (cooling) rate [31].

5.4 Personal Learning Outcomes and Reflections

Besides theoretical learning about the UHI effect and its contributing factors, this project gave me a lot of practical knowledge as well. Since the device is based on AS7341 spectral sensors, I learned about spectroscopy principles, and calibrating for broadband albedo helped me understand the concept of solar irradiance. During testing, I also got some experience with the concept of emissivity while correlating albedo to Land-Surface Temperature (LST).

Coding the device on Arduino IDE improved my skills in C++, while Python was used to obtain the weights for the albedo of each band. This gave me experience with useful data analysis tools and the use of the NumPy, Pandas, and Matplotlib packages for calculations and visualisations. The data for temperature across the day was plotted using Excel, giving me some practice with this tool as well.

5.5 Challenges Faced and Problem-Solving Approach

The most significant challenge experienced was the high cost of equipment for research related to Urban Heat Islands, which prompted most of the innovation in this design. Measuring albedo, an essential task, required a costly albedometer. Thus, I shifted the project's focus towards designing a cheaper one. Early attempts to find broadband albedo, involving dividing the sum of reflected light readings by the sum of incident light readings, failed. This made me aware of the need for proper NTB conversion. However, calibrating the sensor was also an expensive task using traditional methods, which required the original equipment and extensive measurements for regression [9]. I felt that an approach based on the physical irradiance of the solar spectrum would be effective. Thus, the ASTM G-173 dataset was implemented and this novel technique of calibration was tested. Testing the device was also a challenge due to the prohibitive cost of acquiring pure white reference standards, such as Spectralon or Barium Sulphate paint. Thus, I decided to try using common surfaces of known albedo, such as copper and aluminium sheets, a concrete road, and grass in a park near my home. Since albedo is a relative term, sufficient accuracy could be achieved using this method. A second critical challenge arose in accurately measuring Land-Surface Temperature (LST) using an affordable infrared (IR) thermometer, which assumes a fixed emissivity of 0.95. This introduces significant error when measuring materials with low or variable emissivity, such as polished metals. This limitation prompted the practical solution of applying a small square of matte masking tape to the target surface before measurement.

Section 6

6.1 Bibliography

[1] ScienceDirect Topics, "Urban heat island effect," *ScienceDirect Topics*. [Online]. Available: https://www.sciencedirect.com/topics/engineering/urban-heat-island-effect

[2] ResearchGate, "Albedo," *ResearchGate*. [Online]. Available: https://www.researchgate.net/publication/242547003_Albedo

[3] ScienceDirect, "Remote sensing study of urban heat island effect on albedo," *ScienceDirect*. [Online]. Available: https://www.sciencedirect.com/science/article/abs/pii/S1001074208600194

[4] World Bank Data, "Urban population (% of total)," *World Bank Data*. [Online]. Available: https://data.worldbank.org/indicator/SP.URB.TOTL

[5] U.S. Environmental Protection Agency, "Learn about heat island effects," U.S. EPA. [Online]. Available: https://www.epa.gov/heatislands/learn-about-heat-island-effects

[6] ScienceDirect, "Design of a low-cost mobile multispectral albedometer with geopositioning and absolute orientation," *ScienceDirect*. [Online]. Available: https://www.sciencedirect.com/science/article/pii/S2468067222000694

[7] Kipp & Zonen, "Novel estimation of albedo using a drone pyranometer," *Kipp & Zonen*. [Online]. Available: https://www.kippzonen.com/News/803/Novel-Estimation-of-Albedo-Using-a-Drone-Pyranometer

[8] "AS7341 Datasheet," SparkFun, [Online]. Available: https://cdn.sparkfun.com/assets/0/8/e/2/3/AS7341_DS000504_3-00.pdf

[9] MDPI Remote Sensing, "Satellite albedo estimation in complex urban environments," *MDPI Remote Sensing*. [Online]. Available: https://www.mdpi.com/2072-4292/10/1/101

[10] ISO / ITEH, "ISO 9060:2018," *ISO / ITEH*. [Online]. Available: https://cdn.standards.iteh.ai/samples/67464/8a4f719696624455b8bb2b071e5389d6/ISO-9060-2018.pdf

[11] Hukseflux, "How to measure albedo—Best practices," *Hukseflux*. [Online]. Available: https://www.hukseflux.com/library/how-to-measure-albedo-best-practices

[12] Espressif Docs, "Low-power mode (ESP32-C3)," *Espressif Docs*. [Online]. Available: https://docs.espressif.com/projects/esp-idf/en/stable/esp32c3/api-guides/low-power-mode/low-power-mode-soc.html

[13] MikroE, "I2C MUX 5 Click," *MikroE*. [Online]. Available: https://www.mikroe.com/i2c-mux-5-click

[14] ScienceDirect Topics, "Planck constant," *ScienceDirect Topics*. [Online]. Available: https://www.sciencedirect.com/topics/engineering/planck-constant

[15] MDPI Remote Sensing, "Albedo retrieval from unmanned aerial vehicle (UAV) multispectral imagery," *MDPI Remote Sensing*. [Online]. Available: https://www.mdpi.com/2072-4292/12/14/2214

[16] NREL, “Solar spectra AM1.5,” *NREL*. [Online]. Available: https://www.nrel.gov/grid/solar-resource/spectra-am1.5

[17] pvlib-python Documentation, “ASTM G173 spectrum example,” *pvlib-python Documentation*. [Online]. Available: https://pvlib-python.readthedocs.io/en/latest/gallery/spectrum/plot_standard_ASTM_G173-03.html

[18] Antpedia, “ASTM G173-2003 standard,” *Antpedia*. [Online]. Available: https://img.antpedia.com/standard/pdf/A60/1703/ASTM%20G173-2003e1.pdf

[19] MathWorld, “Gaussian function,” *MathWorld*. [Online]. Available: https://mathworld.wolfram.com/GaussianFunction.html

[20] ResearchGate, “Gamma ray modifications of optical-chemical properties of polycarbonate polymer,” *ResearchGate*. [Online]. Available: https://www.researchgate.net/publication/281535907_g_-Ray_Modifications_of_OpticalChemical_Properties_of_Polycarbonate_Polymer

[21] “Sunlight,” *Wikipedia*, Nov. 14, 2025. [Online]. Available: https://en.wikipedia.org/wiki/Sunlight

[22] Fluke / BergEng, “Emissivity chart,” *Fluke / BergEng*. [Online]. Available: https://www.bergeng.com/mm5/downloads/fluke/Emissivity-Values-of-Common-Materials-Chart.pdf

[23] ThermoWorks, “Emissivity table,” *ThermoWorks*. [Online]. Available: https://www.thermoworks.com/emissivity-table/

[24] AMS Journals, “Surface albedo estimation from satellite observations using an improved algorithm,” *AMS Journals*. [Online]. Available: https://journals.ametsoc.org/view/journals/apme/49/8/2010jamc2356.1.xml

[25] MDPI Environments, “A review of urban albedo measurements and modeling,” *MDPI Environments*. [Online]. Available: https://www.mdpi.com/2076-3298/8/10/105

[26] MDPI Sensors, “Low-cost wireless sensor network for urban heat island monitoring,” *MDPI Sensors*. [Online]. Available: https://www.mdpi.com/1424-8220/21/6/1961

[27] MDPI Sustainability, “Albedo and its role in sustainable urban development,” *MDPI Sustainability*. [Online]. Available: https://www.mdpi.com/2071-1050/15/14/10767

[28] MDPI Buildings, “Mitigating urban heat island effect through high albedo materials,” *MDPI Buildings*. [Online]. Available: https://www.mdpi.com/2075-5309/15/5/685

[29] A for Energy, “Bifacial solar panels,” *A for Energy*. [Online]. Available: https://www.aforenergy.com/bifacial-solar-panels-everything-you-need-to-know

[30] Fluke Process Instruments, “Emissivity of metals.” Available: https://www.flukeprocessinstruments.com/en-us/service-and-support/knowledge-center/infrared-technology/emissivity-metals

[31] ScienceDirect Topics, “Normalized difference vegetation index,” *ScienceDirect Topics*. [Online]. Available: https://www.sciencedirect.com/topics/agricultural-and-biological-sciences/normalized-difference-vegetation-index

[32] Sandia PVPMC, “POA ground-reflected irradiance and albedo,” *Sandia PVPMC*. [Online]. Available: https://pvpmc.sandia.gov/modeling-guide/1-weather-design-inputs/plane-of-array-poa-irradiance/calculating-poa-irradiance/poa-ground-reflected/albedo

[33] MDPI Remote Sensing, “Comparison of various methods for urban surface albedo estimation,” *MDPI Remote Sensing*. [Online]. Available: https://www.mdpi.com/2072-4292/9/12/1299

[34] MDPI Sustainability, “Remote sensing of urban heat island and its mitigation strategies,” *MDPI Sustainability*. [Online]. Available: https://www.mdpi.com/2071-1050/13/4/2253

[35] J. S. Botero-Valencia, M. Mejia-Herrera, and J. M. Pearce, “Design and implementation of 3-D printed radiation shields for environmental sensors,” HardwareX, vol. 12, 2022. Available: https://www.sciencedirect.com/science/article/pii/S2468067222000128